DEM Model Calibration for Vertical Filling: Selection of adequate Trials and Handling Randomness

Stefan Kirsch[1*]

[1] Robert Bosch Packaging Technology B.V.

Abstract
The Discrete Element Method (DEM) has been shown to be a viable tool for virtual testing and design optimization of industrial processes, including vertical filling of macroscopic granular foods. In practice, the DEM often relies on model calibration, where parameters are found via iterative adjustment to reproduce observations from experiments with the bulk good. Various calibration trials have been suggested, such as the well-known angle of repose test and bulk discharge from a funnel. However, there is no certainty that the parameters hold up in simulations of the actual process. One further challenge is quantitative model validation.
In this study, we assess existing and original trials for DEM model calibration for a vertical fill process of granular food. Both, the sensitivity to model parameters, as well as to physical randomness were considered. The trials were then employed for iterative DEM model calibration. The calibrated model was then quantitatively validated by comparing the simulations to experiments.

Keywords: Vertical Filling, Granular Foods, Discrete Element Method (DEM), model calibration, noisy optimization, metamodel

*Contact: stefan.kirsch2@bosch.com, stefankirsch@posteo.de

1 Introduction

1.1 Vertical filling

As a broadly deployable and well established process, vertical filling is commonly used in industrial packaging of granular foods, such as candy, snacks and bakery goods. The process is shown schematically in Figure 1. By increasing the frequency of drops of granulate portions, the output rate can be easily increased. However the time distance between the portions must be kept large enough so that there is enough time to perform sealing. Otherwise, a particle might get caught between the sealing jaws, which often results in need for downtime and maintenance. Thus, good machine design and suitable operational settings, that ensure a compact fall of the portions are important for keeping the process economical.

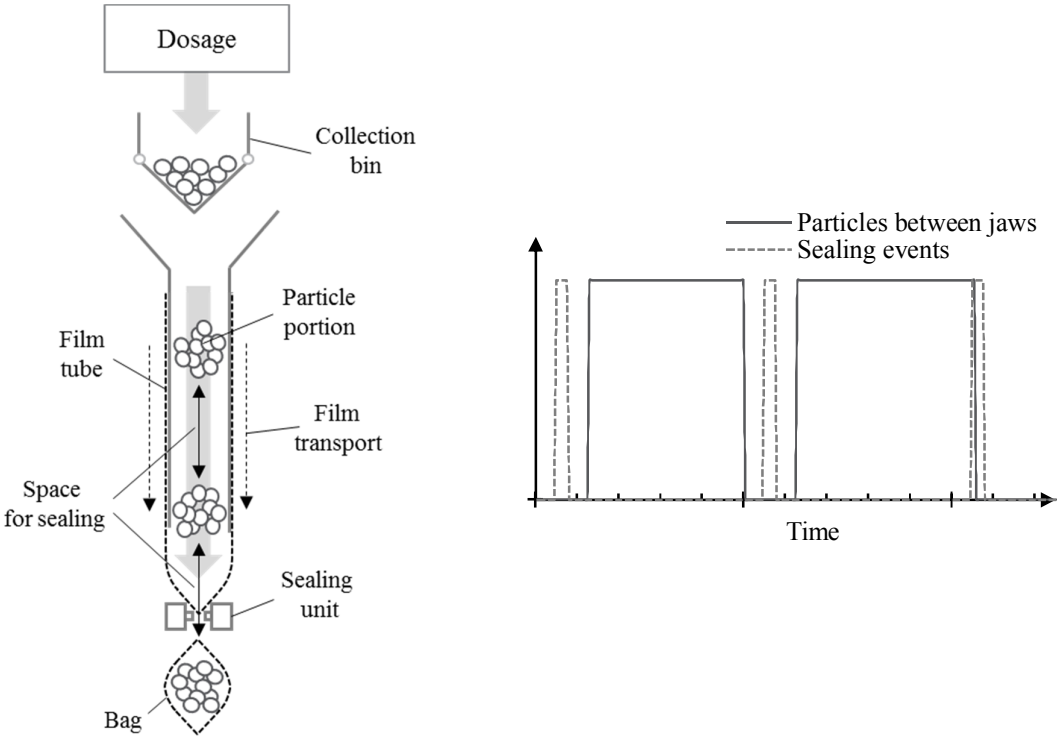

Figure 1: The vertical filling process. (a) Schematic overview over process principle. (b) Successful sealing (left) and likely defect due to particles getting caught in the sealing unit (right)

1.2 Discrete Element Method (DEM)

Overview The physics of granular dynamics are relatively complex and cannot be handled numerically in full detail. The Discrete Element Method (DEM) simplifies contacts by assuming all particles to be stiff. Deformation during contact is implemented by allowing a small overlap between particles. Contact forces are then calculated with simple relations with the current overlap. Figure 2 shows the overlap-force relation according to the linear hysteresis model developed by Walton and Braun [1, 2], as described in [3] and [4]. A variety of other contact models are available in other DEM implementations.

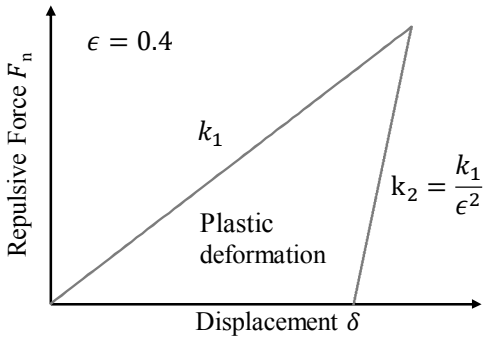

Figure 2: Relationship between particle overlap δ and force F_n for restitution coefficient ε=0.4 (from [4])

Model Calibration Identifying model parameters for DEM simulations is often challenging [5], so often times more or less viable heuristics are used to obtain the desired numerical values [6]. An attractive and commonly used method is numerical model calibration, which consists of varying the model parameters while comparing the simulations to experimental results until reality is reproduced to a satisfactory extend. While there is no universally robust standard procedure available [7], calibration is usually performed in a relatively simple representative experiment [8]. A consecutive validation step can be then performed to verify if the model parameters hold up in the actual process of interest.

Solver Noise A rarely discussed topic with regard to DEM simulations is randomness and associated solver noise. Since granular systems are highly chaotic, small variations in initial conditions (such as the precise positions of individual particles in the collection bin before the drop [4]) can dramatically affect the process outcome [9]. Physical randomness can, just as process design, be of great importance in achieving a desirable outcome and avoiding unfavorable ones. This is true for the physical process as well as the simulations. A second source for uncertainty in the simulations is the so called numerical noise which is a result of random rounding errors in processing of variables that are stored with limited precision in computer memory. Numerical noise is always present, but will be constant if the simulations are performed on a single processor core [10, 11].

1.3 Goal

For this study, model parameters were to be found for a granular sample food. The good chosen was sugar-coated, bite-size chocolate candy with a porous cookie core. Two calibration trials where used, one being a test already used by other groups and one being a drop test that is very similar to the industrial process (representing in-situ calibration [6]). Secondly, the necessity to incorporate the physical randomness in the DEM simulations and their effect on the calibration was evaluated. Finally, the methods were compared with regard to their feasibility, robustness and accuracy.

2 Experimental

2.1 Drop Test

The drop setup has been described in [4] and is shown in Figure 3. Two rectangular falling tubes with different inner areas $A_{\square,1}$ and $A_{\square,2}$ where available. By varying the sample mass, a total of three scenarios were performed (Table 1).

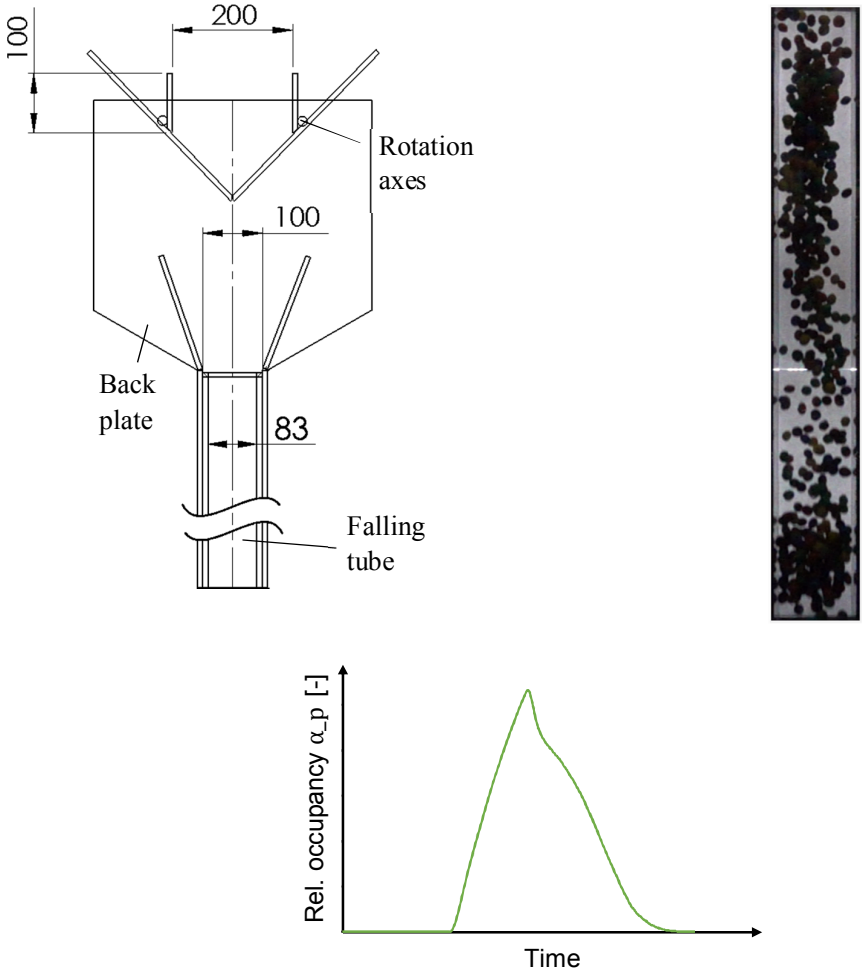

Figure 3: Drop setup described in [4] and snapshot of drop test. Measures in mm.

Sample mass	Inner tube area	Used for
500g	$A_{\square,1}$=76 cm²	Calibration, Validation [1]
	$A_{\square,2}$=100 cm²	Validation[1,2]
700g	$A_{\square,1}$=76 cm²	Validation[1,2]

1 Validation of hopper discharge calibration 2 Validation of drop test calibration

Table 1: Scenarios of the drop test

The experiment was initiated by opening the flaps at the bottom of the sample container. The time stamps of the first and last particle leaving the tube at the bottom were recorded. The difference between these residence times Δt_{res} is equivalent to the portion range τ_{rg} discussed in [4].

$$\tau_{rg} = \Delta t_{res} = \mathrm{t}_{\mathrm{res,lp}} - t_{\mathrm{res,fp}}$$

Secondly, the degree of filling α_p of the tube was tracked over time and normalized to the maximal possible value (entire tube filled). Figure 3 shows a frame cropped to the tube and the relative particle occupancy α_p plotted over time.

2.2 Hopper Discharge

Discharge tests are popular for DEM model calibration [6, 12, 11], since they are fairly simple and can be automated to a great extent. For this study, a Polycarbonate (PC) hopper with a base of 10 cm x 10 cm that could be opened to initiate discharge, was used. The angle of the sides was 45°.
The hopper was filled with 2 kg of candy. Then the bulk surface was flattened to the horizontal as much as possible to reduce random variation. The false floor was then opened and the occupancy α_p was tracked over time. Figure 4 shows a snapshot of the process and the discharge curve normalized to the initial vale of α_p.

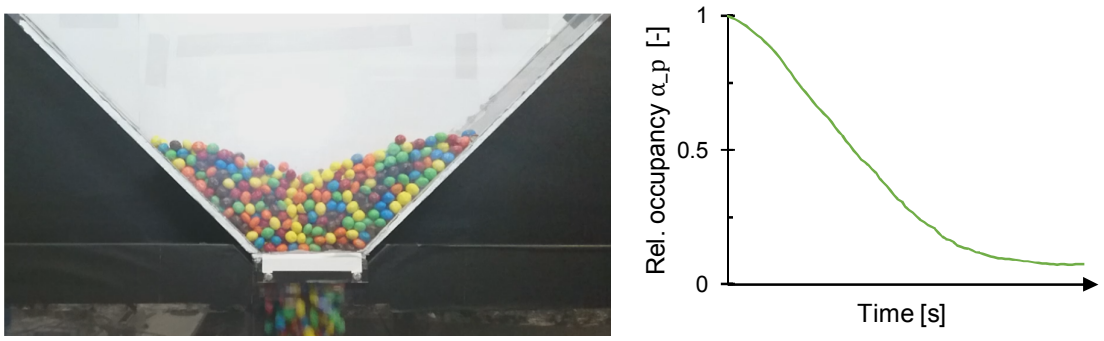

Figure 4: Snapshot of hopper discharge experiment and relative particle occupancy α_p over time

3 Simulation

3.1 Discrete Element Method

The experimental designs from Section 2 were replicated with CAD tools and imported into the DEM environment. The DEM implementation used here features the aforementioned linear hysteresis contact model. The pieces of candy were ellipsoid but nearly spherical, so a spherical particle representation was chosen. The average sieve diameter of the ellipsoids was used as the sphere's diameter.
Gravity driven flows tend to be insensitive to contact stiffness [13], so Young's modulus was chosen with regard to numerical criteria (computational cost and numerical stability) and left constant at 10^8 Pa. The calibration parameters x (Table 2) were friction coefficients μ, respectively for the static (sticking) and the dynamic (sliding) case and the coefficients of restitution ϵ. Each parameter was assumed different for the interaction between the particles (P-P) and the interaction between particles and the boundary (P-B). Additionally, a factor for rolling resistance was employed to account for the increased rolling of spherical particles compared to the real particles [12].
The eventual model parameters x differ from the "true" physical parameters due to model shortcomings [14, 15]. For the raw model, i.e. the start values of the calibration, literature values where used. Since limited data for sugar coating is available in literature, rice was chosen as a stand-in. The static friction $\mu_{s,P-B}$ between particle and boundary was calculated from the angle θ_{max} where sliding starts, measured in an inclined plane test.

$$\mu_{s,P-B} = \tan \theta_{max}$$

With dynamic friction between particles $\mu_{d,P-P} = 0$ [16], the simulations occasionally showed unrealistic behavior when a particle was compressed between other particles (soap bar effect). $\mu_{d,P-P}$ was therefore set to 0.1. The start value for RR was estimated at 0.1.

Parameter	Material and Scenario		Symbol	Start Values (Raw Model)
Friction	Particles – Particles	Static	$x_1 = \mu_{s,P-P}$	0.8 [17] (Rice-Rice)
		Dynamic	$x_2 = \mu_{d,P-P}$	0.1 (Numerical Stability)
	Boundary - Particles	Static	$x_3 = \mu_{s,P-B}$	0.45 (Experimental)
		Dynamic	$x_4 = \mu_{d,P-B}$	0.1 [16] (Sugar Coating-PC)
Restitution	Particles – Particles		$x_5 = \epsilon_{P-P}$	0.1 [17] (Rice-Rice)
	Boundary - Particles		$x_6 = \epsilon_{P-B}$	0.1 [17] (Rice-Celluloid)
Rolling Resistance	Particles		$x_7 = RR$	0.1 (Estimated)

Table 2: Calibration Parameters

3.2 Calibration

The goal of model calibration is to identify the parameter set x that produces the best match between the simulations w and the experimental results u. For the hopper discharge test, the curves from simulation and experiment should be matched, i.e. the point-wise difference $\Delta_{\mathrm{pw}}\alpha_p$ should become 0. [11] In the case of the drop test, we aim to reproduce the portion range τ_{rg} from the experiment as accurately as possible. These goals can be formulated as optimization problems, where the error between simulation and experiment is to be minimized. Several optimization strategies have been used for DEM model calibration, such as manual comparison [11], gradient-based methods [18], genetic algorithms [19] and Artificial Neural Networks [5]. A recently followed approach is to create a metamodel with a kriging algorithm from several representative anchor points in the parameter space. The optimization can then be performed on the resulting surrogate model [20].The benefit of the latter method is that the number of solver runs can be reduced and evaluation of the goal function on the surrogate model is quick.
The procedure was implemented in an automated calibration workflow (Figure 5) in the optimization environment optiSLang. The DEM solver was called at different parameter sets (samples) and the results were compared against the experimental data. The data was then processed into a metamodel of the solver behavior.

Metamodelling A metamodel is a model for a model, in this case an approximation of the solver result w which in turn attempts to model experimental observations u. Kleijnen [21] gives a comprehensive theoretical overview over metamodelling techniques, so we will use part of his nomenclature here. The solver output w is to be approximated by the output $\widehat{w}$ of the metamodel f_{meta}.

$$w = f_{sim}(x, r) = f_{meta}(x) + e$$

f_{sim} is the noisy solver function which depends on the calibration parameters x and the seed of the random number generator r. The metamodel function is f_{meta} with its value depending only on the calibration parameters x. e is the residual vector, in which the local error of the metamodel at anchor point i is

$$e_i = \widehat{w}_i - w_i$$

If we make the assumption, that the kriging algorithm is capable of describing the behavior of a deterministic solver $f_{sim}(x)$, there must be an kriging parameter set β which provides optimal fidelity. However, we must keep in mind, that we only have a finite amount of anchor points n to work with, so we can in turn only find an estimate $\hat{\beta}$ of β. The sample size n can be increased at any time, resulting in

the residuals e asymptotically decreasing until an acceptable accuracy is reached at which the process is finalized. [21]

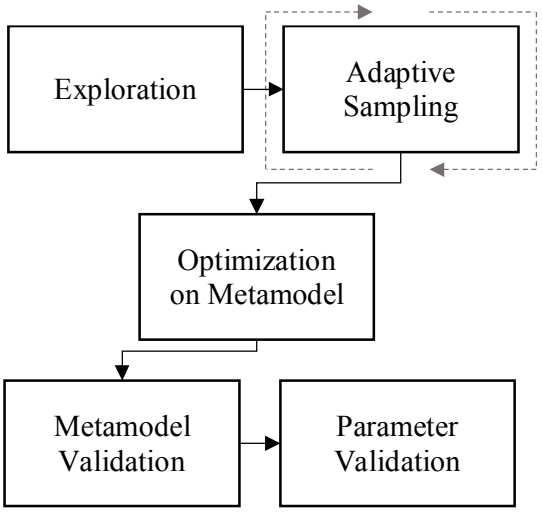

Figure 5: Calibration Workflow in optiSLang

In the case of a noisy solver $f_{sim}(z, r)$, the regression will smooth out some of the solver noise [22, 21], while producing greater residuals than in the deterministic case. This however does not necessarily imply bad quality of the metamodel but rather highlights the deterministic nature of f_{meta}. It should be noted that, in the noisy case, the criterion, after how many simulation run the metamodel should be finalized, is not obvious. A possible criterion is to track the mean residuals over the number of anchor points n and stop the process when stagnation is reached. It is however not guaranteed that this point will coincide with an acceptable quality of $\hat{\beta}$.

Adaptive Sampling Choosing the anchor points with Latin Hypercube sampling (LHS) [23, 24] allows for good coverage of the parameter space while avoiding undesired sampling effects at a smaller number of anchor points [25]. However DEM simulations are computationally expensive, so adaptive sampling, similar to [26], was performed to reduce the required number of solver calls.
The general topology (i.e. global trends) of the metamodel can be estimated quite well in an exploration phase with relatively coarse sampling. In order to refine the metamodel, we can add anchor points in the interesting regions of the metamodel, i.e. where the predicted error $\Delta\tau_{rg}$ between simulation w and experiment u is low. The refinement is fully automated in optiSLang: First a series of preliminary optimizations is initialized at different starting points. With the resulting information on interesting regions on the metamodel, an 'expected improvement approach' [27] is employed to select additional anchor points. The solver is then executed at the new anchor points and the metamodel is recalculated with all anchor points available. The metamodel refinement is repeated for several iterations until a finalization criterion is met (in this case stagnation of the residuals) or the maximum computation budget is spent.

Optimization Kriging models are continuous and smooth, so fast gradient based approaches can be used for optimization [26, 28]. The implementation the Lagrangian NLPQL solver of optiSLang was used due to its numerical performance and accuracy [29, 30].

3.3 Validation

There are two sources for errors in the calibration process: Numerical (insufficient metamodel quality) and systematic (measurement errors and shortcomings in the DEM model). To exclude both, two separate validation steps were performed.

Metamodel Validation In order to ensure the prediction capability of the metamodel, a set of m validation simulation runs were performed at the supposed minimum x_{opt} and their results $w_1, w_2, \dots, w_m$ were averaged to $\overline{w}_{opt}$. The difference $e_{opt} = \hat{w}_{opt} - \overline{w}_{opt}$ is a teller for the reliability of the metamodel at that respective point. If the error is unacceptably high, more anchor points should be added to increase the accuracy of $\hat{\beta}$.

Parameter Validation To verify that the obtained parameter set x_{opt} was viable outside the calibration scenario, validation simulations were performed in the respective scenarios shown in Table 1. The respective results were obtained from m averaged simulation runs.

Randomness In real-life, the filling of the containers is a random process that cannot be reproduced in the next run, resulting in a partially random initial condition (RIC) of the bulk. This randomness is a physical property of the processes, influencing the outcome of the experiment. The DEM simulations can either be performed with a RIC, accounting for physical randomness or with an arbitrary constant initial condition (CIC), with only numerical noise.
Figure 6 shows the histogram of a set of noisy simulations of the drop test from Section 2.1 with the raw model. (a) shows the case of a constant initial condition (CIC). The only source of randomness here was numerical noise, since the simulations were performed on 8 processor cores. (b) shows the respective simulation with the aforementioned random initial condition.
Neglecting physical randomness has the potential to lead to a biased result of the calibration, depending on how much the particular initial condition chosen affects the process outcome. The simulations were thus performed with physical randomness: Both in the drop test and the hopper discharge, a random and flat particle bed was created in the simulations before release, ensuring a RIC.

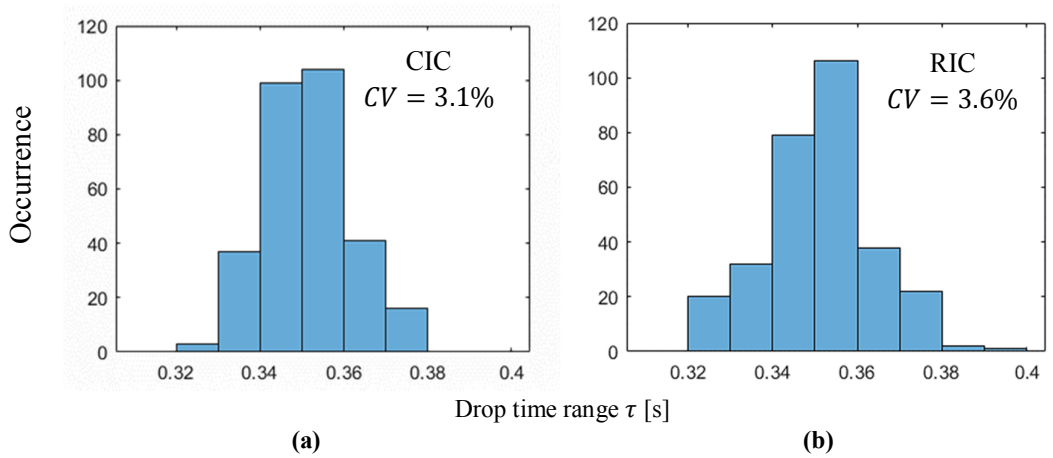

Figure 6: Histograms of simulations of the drop test with the ram model and 500 g of particles with constant initial state (a) and random initial state (b)

Creating the RIC adds computational cost: in the case of the drop 37 seconds to the runtime of 110 seconds per run on average (34%). Furthermore, the RIC increases solver noise.
Both increased cost and solver noise are undesirable from an engineering standpoint. Since the difference in the relative standard deviation (coefficient of variation) CV between CIC and RIC is low, it is unclear if the physical randomness actually plays a significant role and that the additional effort will yield in higher fidelity models. In order to determine whether the implementation of the physical randomness is actually necessary, for the drop test, we also performed the calibration with an arbitrary but constant initial state (CIC).

4 Results

4.1 Drop Calibration

Table 3 shows the number of anchor points (simulated parameter sets) over the iterations. Figure 7 shows a projection of a graphical representation of the metamodel after iterations 1 and 10 respectively. The parameters found to be the most influential on the portion range τ_{rg} were $\mu_{d,P-B}$ and RR. All other parameters are held constant near their respective optimum for low DEM model error. We observe only a slight change in the topology of the metamodel between Iteration 1 and 10. This suggests that the sampling could be stopped after iteration 1.

	Iteration 1 (Exploration)	Iteration 3	Iteration 10	Iteration 20	Average per Iteration*
n_{RIC}	290	379	693	1162	46
Comp. cost	11.8 h	15.4 h	28.2 h	47.3 h	1.9 h
n_{CIC}	289	378	698	1143	45
Comp. cost	9.1 h	11.5 h	21.3 h	34.9 h	1.4 h

*after iteration 1

Table 3: Number of anchor points n and total computational cost of the calibration in the drop test at different iterations, depending on whether the RIC or CIC is simulated

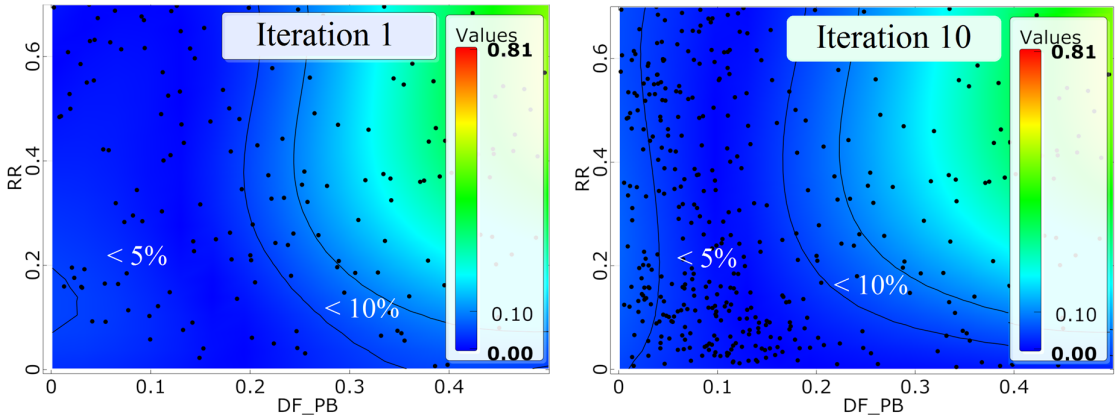

Figure 7: 2-dimensional projection of the 7-dimensional metamodel for $\Delta\tau_{rg}$ in % in relation to the two most influential parameters (RR and $\mu_{d,P-B}$) at iteration 1 (Exploration) and 10 (RIC)

However, to gain insight into the quality of the prediction of the metamodel, we must also assess the residuals e of $\Delta\tau_{rg}$. Figure 8 shows the local residuals e of the metamodel in the same range as Figure 7. We find that uncertainty is quite high at iteration 1, especially in the area of low predicted errors $\Delta\tau_{rg}$. This implies a bad estimate $\hat{\beta}$. After increasing the number of anchor points to more than twice the original count, at iteration 10, residuals were significantly lower, especially in the interesting areas of the metamodel.

Figure 9 shows the relationship between the residuals e in regions of low predicted errors $\Delta\tau_{rg}$ and iteration number for the entire parameter space. Stagnation begins after iteration 3, which suggests that adding samples does not improve the metamodel anymore [21].

In the next step the minimum error $\min(\Delta\tau_{rg})$ was determined on the metamodel with the NLPQL optimizer. The runtime was < 1 min. The metamodel was then validated at the supposed minimum x_{opt}

according to Section 3.2, showing a very good match (Figure 10). This confirms that the metamodel is indeed of high quality.

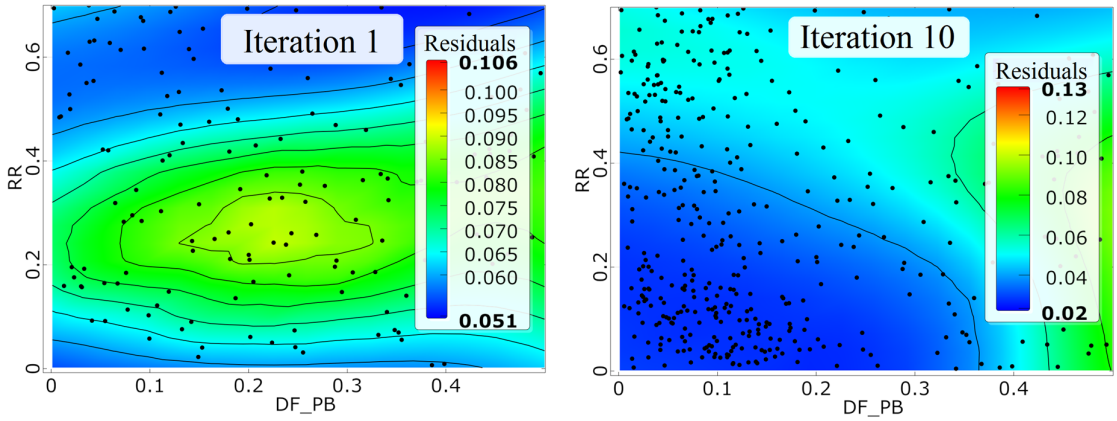

Figure 8: 2-dimensional projection of the local residuals e of $\Delta\tau_{rg}$ for iteration 1 (exploration) and iteration 10 (RIC)

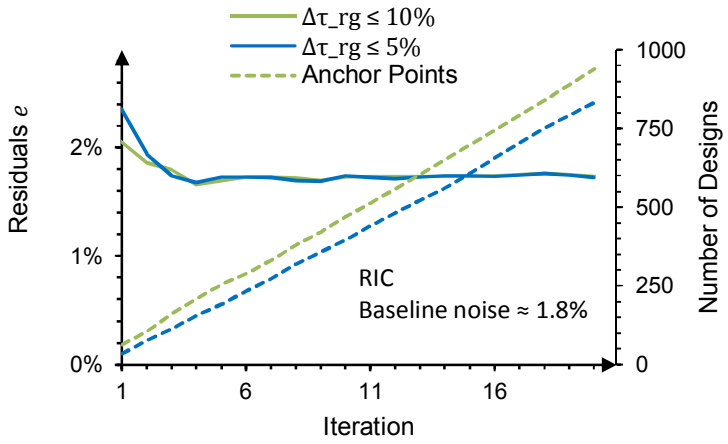

Figure 9: Residuals e of τ_{rg} for the areas of the metamodel with low predicted DEM model errors $\Delta\tau_{rg}$ over iterations (RIC). The respective number of iteration used to calculate the residuals are shown as dotted lines.

The optimized parameter set x_{opt} was then used for the two validation trials laid out in Section 3.3. The results are shown in Figure 10. We find that the calibrated model exhibits a high fidelity in reproducing the experimental results. An overview over the accuracy of the DEM models is presented in Table 4. The entire calibration process was repeated with a constant initial condition (CIC) before the drop. The results are shown in Figure 10. We obtain an equally good result as in the case with the RIC. We conclude that in this case, the physical randomness was not crucial for the accuracy of the metamodel. It should be noted however, that this could only be true for the specific arbitrary CIC chosen here. Other initial conditions might still produce a biased metamodel.

4.2 Hopper Calibration

The results of the calibration in the hopper discharge experiment are shown in Figure 11. The validation shows an equally good match as in the case of the calibration in the drop test.

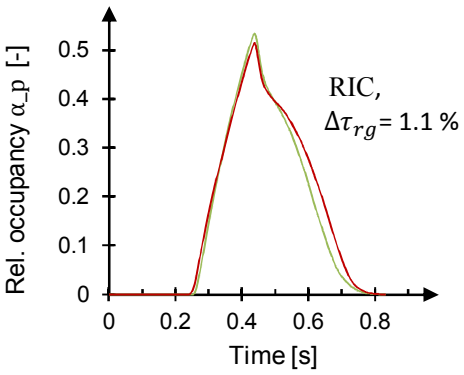

RIC, 500 g, $A_{\square,1}$ (Metamodel Validation)

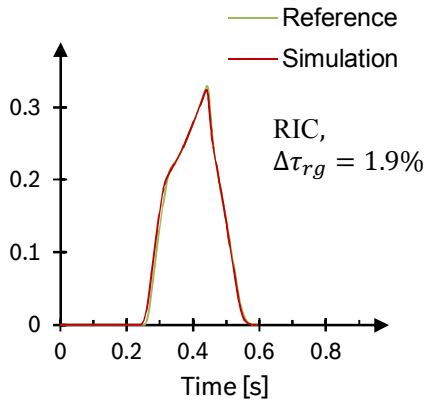

RIC, 500 g, $A_{\square,2}$ (Parameter Validation)

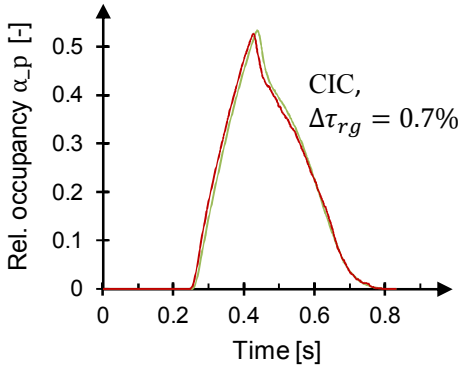

CIC, 500 g, $A_{\square,1}$ (Metamodel Validation)

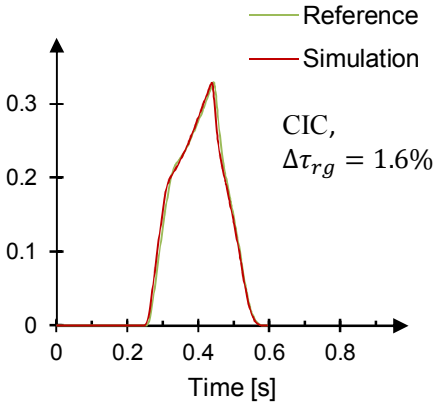

CIC, 500 g, $A_{\square,2}$ (Parameter Validation)

Figure 10: Results of calibration in the drop test (RIC and CIC).Validation of metamodel after optimization and parameter validation in the drop test with $A_{\square,2} > A_{\square,1}$

m=20	Metamodel Validation	Parameter Validation		
		500 g, $A_{\square,1}$	500 g, $A_{\square,2}$	700 g, $A_{\square,1}$
Drop, RIC	$\Delta\tau_{rg} = 1.1\%$	-	$\Delta\tau_{rg} = 1.9\%$	$\Delta\tau_{rg} < 0.1\%$
Drop, CIC	$\Delta\tau_{rg} = 0.7\%$	-	$\Delta\tau_{rg} = 1.6\%$	$\Delta\tau_{rg} = 0.7\%$
Hopper discharge	$\Delta_{\mathrm{pw}}\alpha_p = 3.8\%$	$\Delta\tau_{rg} = 2.0\%$	$\Delta\tau_{rg} = 1.1\%$	$\Delta\tau_{rg} = 0.4\%$

Table 4: Actual error of τ_{rg} for metamodel validation and for the eventual calibrated parameters x for the random initial condition (RIC), constant initial condition (CIC) and the hopper discharge. Simulations were performed m=20 times and their results averaged.

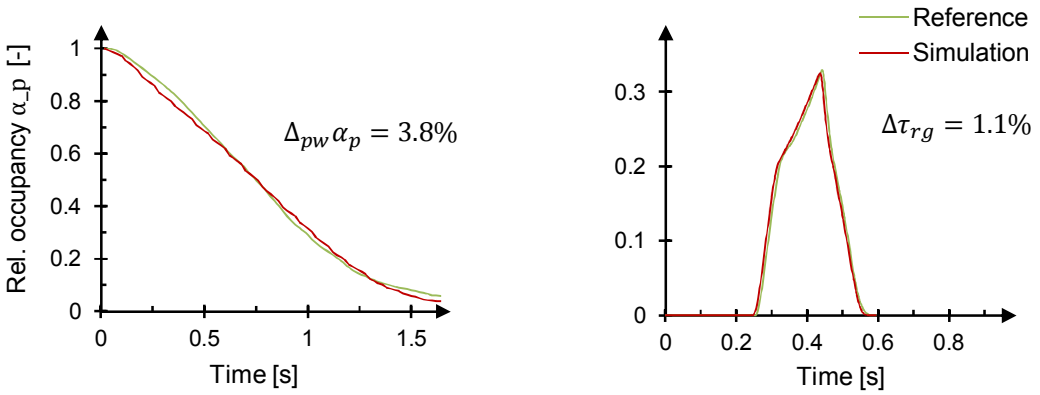

Hopper discharge (Metamodel Validation) 500 g, $A_{\square,2}$ (Parameter Validation)

Figure 11: Results of calibration in the hopper discharge test: Validation of metamodel after optimization and Parameter Validation in the drop test with $A_{\square,2}$

5 Conclusion

We set out to investigate two experimental approaches for DEM model calibration, suitable to identify parameters for the simulation of a drop trial analogous to industrial vertical filling. The first experiment was the drop test itself (in-situ calibration) while the second one was a commonly used hopper discharge test. In this regard, we investigated whether physical noise in the drop test due to the random initial condition at the beginning of the experiment needed to be included in the DEM simulations to obtain a good calibration result.

We found that both experiments are suitable for calibration, yielding low prediction errors of a maximum of 2%. The calibration in the drop test was repeated without physical noise which yielded an equally good result. This suggests the conclusion that physical noise is not relevant for the calibration. However it still needs to be proven whether this is true for all initial conditions or only some.

References

[1] O. R. Walton and R. L. Braun, "Viscosity, granular temperature, and stress calculations for shearing assemblies of inelastic, frictional disks," *Journal of Rheology,* 1986.

[2] S. Luding, "Collisions & Contacts Between Two Particles," *Physics of Dry Granular Media,* vol. 350, pp. 285-304, 1998.

[3] C. Thornton, S. J. Cummins and P. W. Cleary, "An investigation of the comparative behaviour of alternative contact force models during inelastic collisions," *Powder Technology,* vol. 233, pp. 30-46, 2013.

[4] S. Kirsch and A. Philipp, "Simulation of Vertical Filling Processes of Granular Foods for typical Retail Amounts," in *9th Conference Processing Machines and Packaging Technology*, 2018.

[5] L. Benvenuti, C. Kloss and S. Pirkera, "Identification of DEM simulation parameters by Artificial Neural Networks and bulk experiments," *Powder Technology,* vol. 291, pp. 456-465, 04 2016.

[6] C. J. Coetzee, "Review: Calibration of the discrete element method," *Powder Technology,* vol. 310, pp. 104-142, 04 2017.

[7] C. J. Coetzee, "Calibration of the discrete element method and the effect of particle shape," *Powder Technology,* vol. 297, pp. 50-70, 09 2016.

[8] T. Gröger and A. Katterfeld, "On the numerical calibration of discrete element models for the simulation of bulk solids," in *16th European Symposium on Computer Aided Process Engineering and 9th International Symposium on Process Systems Engineering*, Elsevier BV, 2006, pp. 533-538.

[9] T. Shinbrot, "Granular chaos and mixing: Whirled in a grain of sand," *Chaos,* vol. 25, 09 2015.

[10] H. G. Matuttis and J. Chen, Understanding the Discrete Element Method: Simulation of Non-Spherical Particles for Granular and Multi-body Systems, Wiley, 2014.

[11] M. Frank and J. Holzweißig, "Simulation-based optimization of geometry and motion of a vertical tubular bag machine," *Sächsische Landesbibliothek,* 03 2016.

[12] D. Markauskas and R. Kačianauskas, "Investigation of rice grain flow by multi-sphere particle model with rolling resistance," *Granular Matter,* vol. 13, pp. 143-148, jul 2010.

[13] Y. Xu, K. D. Kafui, C. Thornton and G. Lian, "Effects of material properties on granular flow in a silo using DEM simulation," *Particulate Science and Technology,* vol. 20, pp. 109-124, 04 2002.

[14] C. González-Montellano, J. M. Fuentes, E. Ayuga-Téllez and F. Ayuga, "Determination of the mechanical properties of maize grains and olives required for use in DEM simulations," *Journal of Food Engineering,* vol. 111, pp. 553-562, 08 2012.

[15] X. Huang, "Exploring critical-state behaviour using DEM," 2014.

[16] B. C. Hancock, N. Mojica, K. St.John-Green, J. A. Elliott and R. Bharadwaj, "An investigation into the kinetic (sliding) friction of some tablets and capsules," *International Journal of Pharmaceutics,* vol. 384, pp. 39-45, jan 2010.

[17] J. Guowei and Q. Baijing, "Discrete Element Method Simulation of Impact-Based Measurement of Grain Mass Flow," in *2011 International Conference on Computer Distributed Control and Intelligent Environmental Monitoring*, 2011.

[18] M. W. Johnstone, "Calibration of DEM models for granular materials using bulk physical tests," 2010.

[19] H. Q. Do, A. M. Aragón and D. L.Schott, "A calibration framework for discrete element model parameters using genetic algorithms," *Advanced Powder Technology,* vol. 29, pp. 1393-1403, 06 2018.

[20] M. Rackl and K. J.Hanley, "A methodical calibration procedure for discrete element models," *Powder Technology,* vol. 307, 02 2017.

[21] J. P. C. Kleijnen, "Simulation Optimization through Regression or Kriging Metamodels," *Discussion Paper,* 05 2017.

[22] T. Most and J. Will, "Sensitivity analysis using the Metamodel of Optimal Prognosis," in *Weimar Optimization and Stochastic Days*, 2011.

[23] M. D. McKay, R. J. Beckman and W. J. Conover, "A Comparison of three methods for selecting values of input variables in the analysis of output from a computer code," *Technometrics,* vol. 21, pp. 239-245, 05 1979.

[24] J. C. Helton and F. J. Davis, "Latin hypercube sampling and the propagation of uncertainty in analyses of complex systems," *Reliability Engineering and System Safety,* vol. 81, pp. 23-69, 2003.

[25] M. Rackl, C. D. Görnig, W. A. Günthner and K. J. Hanley, "Efficient calibration of discrete element material model parameters using Latin hypercube sampling and kriging," in *ECCOMAS Congress 2016 - Proceedings of the 7th European Congress on Computational Methods in Applied Sciences and Engineering*, 2016.

[26] R. K. Rathore, K. Sharma and A. Sarda, "An Adaptive Approach for Single Objective Optimization," *Int. Journal of Engineering Research and Applications,* vol. 4, pp. 737-746, 02 2014.

[27] D. R. Jones, "A Taxonomy of Global Optimization Methods Based on Response Surfaces," *Journal of Global Optimization,* vol. 21, p. 345–383, 2001.

[28] F. Jurecka, "Automated metamodeling for efficient multi-disciplinary optimisation of complex automotive structures," in *7th European LS-DYNA Conference, Salzburg, Austria*, 2009.

[29] K. Schittkowski, "NLPQL: A fortran subroutine solving constrained nonlinear programming problems," *Annals of Operations Research,* vol. 5, pp. 485-500, Jun 1986.

[30] Y.-h. Dai and K. Schittkowski, "A Sequential Quadratic Programming Algorithm with Non-Monotone Line Search," *Pacific Journal of Optimization,* vol. 4, 2008.